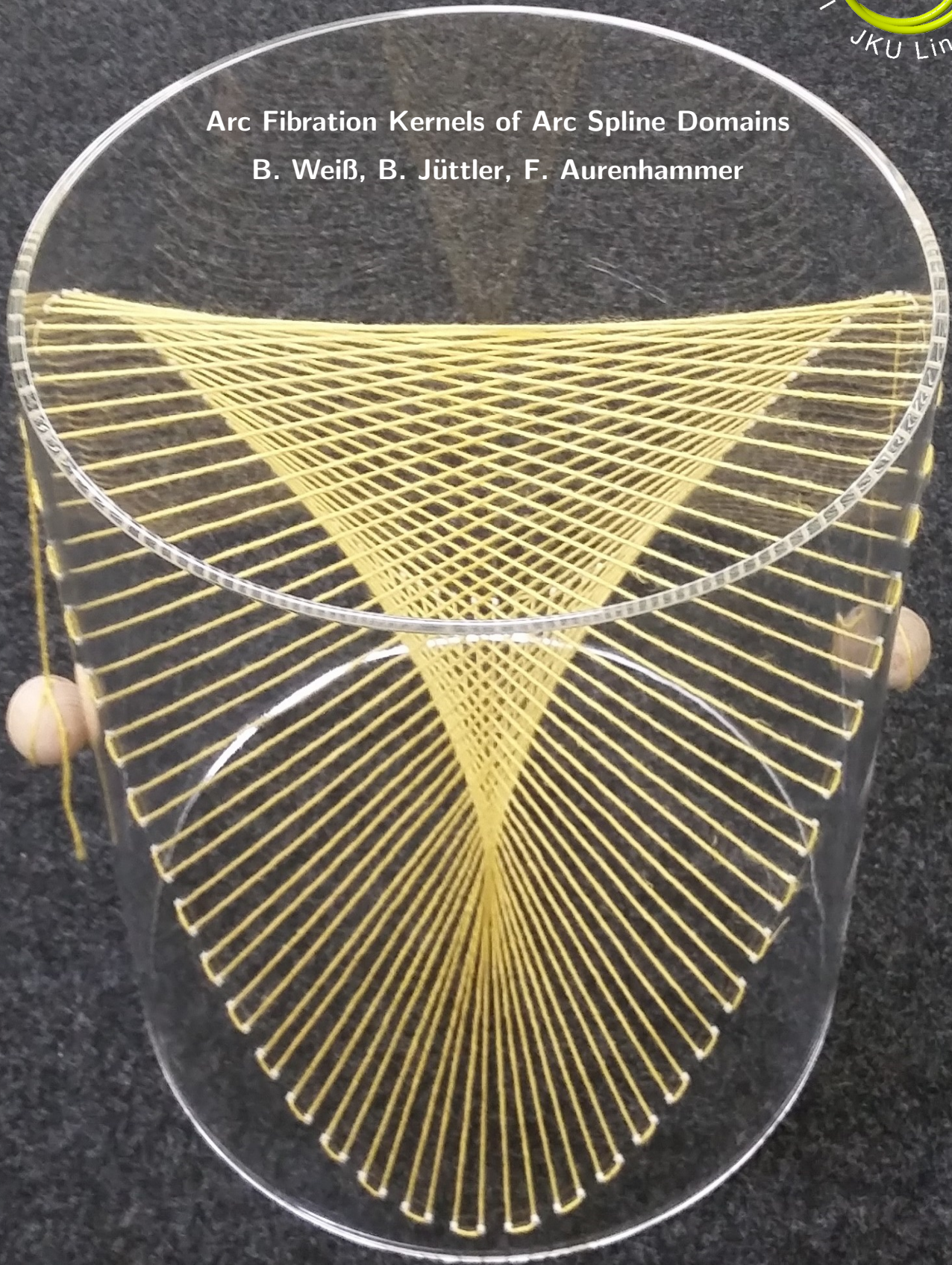


Arc Fibration Kernels of Arc Spline Domains
B. Weiß, B. Jüttler, F. Aurenhammer



Arc Fibration Kernels of Arc Spline Domains

Bastian Weiß, Bert Jüttler and Franz Aurenhammer

Abstract Any star-shaped domain can be parameterized by using a point in its kernel as the center of a polar parameterization. An arc fibration is a regular polar parameterization whose parameter lines are circular arcs. The existence of arc fibrations has been studied recently for domains defined by C^2 -smooth boundary curves. The set of feasible center points forms the arc fibration kernel of a planar domain. We extend these results in two ways: First, the notion of arc fibration is generalized to domains with boundary curves that are only C^1 smooth. These include the class of piecewise circular curves (arc splines), which are of particular interest since they combine computational simplicity with high accuracy. Second, we examine the arc fibration kernel for domains bounded by arc splines. An algorithm is presented that extracts the kernel of such a domain. Its performance is demonstrated by several examples.

1 Introduction

The computation of parameterizations of planar domains, which are defined by their boundary curves, is a fundamental task in geometric modeling, computer graphics, isogeometric analysis, and related fields. A particularly simple solution is available for the class of star-shaped domains, which are characterized by the fact that there exists a center point in the domain's interior that sees all boundary points. The set of all such center points then forms the *kernel* of the domain.

Bastian Weiß and Bert Jüttler
Johannes Kepler University Linz, Institute of Applied Geometry Altenberger Str. 69 A-4040 Linz,
Austria, e-mail: bastian.weiss@jku.at, e-mail: bert.juettler@jku.at

Franz Aurenhammer
Graz University of Technology, Institute of Theoretical Computer Science Inffeldgasse 16b/1 8010
Graz, Austria, e-mail: franz.aurenhammer@igi.tugraz.at

Kernels of polygons are well understood. An optimal algorithm that computes the kernel of a polygon with linear complexity was proposed by Lee and Preparata [8]. Icking and Klein [6] presented a competitive strategy for walking into the kernel of a yet unknown star-shaped polygon. Any polygon can be partitioned into star-shaped polygons in $O(n \log n)$ time, as shown by Avis and Toussaint [3].

Dobkin and Souvaine [4] extended algorithms for straight-edged polygons to polygons with curved edges. Various classical problems, such as convex hull computation, kernel computation and monotonicity testing, are analyzed for curved edge polygons. Aichholzer et al. [2] studied algorithms for the particular class of arc splines, i.e., for piecewise circular curves. These curves provide efficient representations of planar free form shapes. In particular, they are well suited for the computation of offset curves and of the medial axes, see Aichholzer et al. [1]. Mitered offsets of arc polygons (and the associated skeletons) were studied recently by Weiß et al. [13].

Star-shaped domains admit polar parameterizations by straight line segments. Utilizing the more general class of circular arcs as parameter lines leads to the notion of *arc fibrations*, which was introduced by Jüttler et al. [7]. These arc fibrations are available for a wider class of domains that includes star-shaped ones. Similar to the kernel of a star-shaped domain, the *arc fibration kernel* is formed by all points that are suited to serve as center points of an arc fibration. The analogous construction for parabolic arcs was explored recently by Trautner et al. [10].

The contributions of this paper are, on the one hand, the investigation of arc fibrations for arc spline domains, i.e., domains represented by arc spline boundary curves. We will use the notion of *discrete osculating circles* in order to extend the results of [7], which apply to domains with C^2 -smooth boundary curve only, to arc spline domains. On the other hand, we propose a simple geometric algorithm that computes the arc fibration kernel. It will be shown that this kernel possesses a piecewise circular boundary for arc spline domains, which makes it accessible for computations. This is quite different from the case of general boundary curves, which was explored by Jüttler et al. [7].

The remainder of the paper is organized as follows. Section 2 recalls the theoretical foundations of arc fibrations, which were originally established for C^2 smooth boundary curves, and extends to C^1 -smooth arc splines. The φ -channel and arc fibration kernel are introduced and discussed in Sections 3 and 4, respectively. In the subsequent chapter, we develop an algorithm that computes the arc fibration kernel of an arc domain by generating a super-set of its boundary curve elements from which the kernel can be extracted. The algorithm's performance is analyzed by applying it to various arc domains, manually designed ones and approximations of free-form splines in Section 6. Finally, possible extensions and applications of our approach are discussed.

2 Arc fibrations of arc spline domains

We consider a closed, simply connected and bounded domain $\Omega \subset \mathbb{R}^2$ which is defined by a C^1 -smooth boundary curve b such that $\partial\Omega = b$. Therefore, $b(t)$ is a closed and simple curve.

Recall that a function f is *quasi-periodic* with *quasi-period* q and constant D if $f(t+q) = f(t) + D$ holds. This notion also applies to sequences, in which case its elements satisfy $t_{\ell+q} = t_\ell + D$.

An *arc spline* is a C^1 -smooth (with respect to arc-length parameterization), piecewise circular curve. We consider simple, closed curves with positive orientation, which are represented by L -periodic parametric arc spline curves $b : \mathbb{R} \rightarrow \mathbb{C}$, where L denotes the total arc length.

More precisely, for any curve $b(t)$, there exists a strictly increasing bi-infinite quasi-periodic sequence $J = (t_\ell)_{\ell \in \mathbb{Z}}$ of knots $t_\ell \in \mathbb{R}$ with quasi-period n , i.e., $t_{\ell+n} = t_\ell + L$. Each *knot span* $[t_\ell, t_{\ell+1})$ is equipped with a center $m_\ell \in \mathbb{C}$, a signed radius $r_\ell \in \mathbb{R} \setminus \{0\}$ and an angle $\alpha_\ell \in \mathbb{R}$. The condition

$$0 < |\alpha_{\ell+1} - \alpha_\ell| < 2\pi$$

ensures that each arc is traced exactly once. We use consecutive angles α_ℓ and $\alpha_{\ell+1}$ to define

$$\sigma_\ell(t) = \frac{t - t_\ell}{t_{\ell+1} - t_\ell} \alpha_{\ell+1} + \frac{t_{\ell+1} - t}{t_{\ell+1} - t_\ell} \alpha_\ell$$

which is the affine function that satisfies $\sigma_\ell(t_\ell) = \alpha_\ell$ and $\sigma_\ell(t_{\ell+1}) = \alpha_{\ell+1}$. The periodicity of the knots carries over to the centers, radii and angles by

$$m_\ell = m_{\ell+kn}, \quad r_\ell = r_{\ell+kn} \quad \text{and} \quad \alpha_\ell = \alpha_{\ell+kn} \quad \text{for all } k.$$

Choosing the signs of the radii as

$$\text{sign } r_\ell = \text{sign}(\alpha_{\ell+1} - \alpha_\ell) \tag{1}$$

ensures that arcs with positive or negative orientation get a positive or negative radius, respectively. The arc spline thus takes the form

$$b(t) = m_\ell + r_\ell e^{i\sigma_\ell(t)} \quad \text{for } t \in [t_{\ell+kn}, t_{\ell+kn+1}) \quad \forall \ell, k.$$

Its C^1 -smoothness is guaranteed by two conditions: First, we choose the knots such that

$$r_\ell(\alpha_{\ell+1} - \alpha_\ell) = t_{\ell+1} - t_\ell.$$

This causes $b(t)$ to have unit speed everywhere. Second, adjacent centers m_ℓ and $m_{\ell+1}$ satisfy

$$m_\ell + r_\ell e^{i\sigma_\ell(t_{\ell+1})} = m_{\ell+1} + r_{\ell+1} e^{i\sigma_{\ell+1}(t_{\ell+1})}$$

or, equivalently,

$$m_\ell - m_{\ell+1} = (r_{\ell+1} - r_\ell) e^{i\alpha_{\ell+1}}.$$

The transition points between adjacent arcs are called the *joints*, $v_\ell = b(t_\ell)$. The individual arcs of an arc spline are denoted by b_ℓ . *Arc spline domains* are domains with arc spline boundaries. Figure 1 shows the centers, joints and angles that are necessary to describe an arc domain boundary.

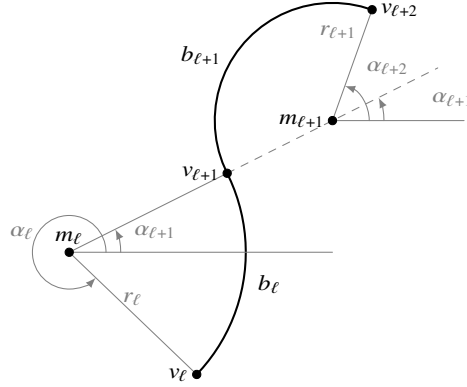


Fig. 1 Two boundary arcs and their associated centers, angles and joints

A polar parameterization of the domain Ω is a continuous mapping

$$p : [0, 1] \times \mathbb{R} \rightarrow \Omega$$

with center $p(0, t) = z$ and $p(1, t) = b(t)$, which is L -periodic with respect to t , $p(s, t) = p(s, t + L)$. In particular, we consider a smooth (i.e., differentiable) polar parameterization by circular arcs where the parameter lines are segments of circles.

Definition 1 An *arc fibration* is a regular (except in the center $z = p(0, t)$) smooth polar parameterization with the property that the parameter lines $p(\cdot, t)$ are circular arcs.

Fig. 2 shows a simple example of an arc fibration. A special case of an arc fibration is the polar parameterization of a star-shaped domain Ω by straight line segments. Such a parameterization exists for any center z in the domain's kernel, but it is not available for non-star-shaped domains. In order to increase the flexibility of this construction, we investigate the possibility to construct a parameterization for a given center point in Ω by using circular arcs as parameter lines. For simplicity we fix the center at the origin, $z = 0$.

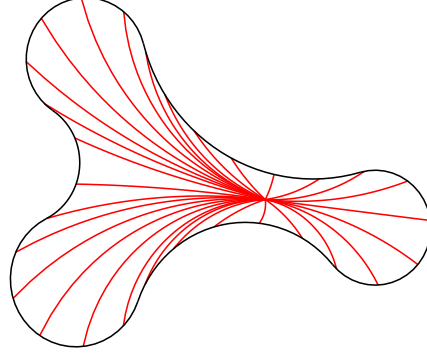


Fig. 2 An arc fibration of a planar domain

According to a result of Zubè [14], the polar parameterization with circular arcs as parameter lines takes the form

$$p(s, t) = \frac{(1-s)b(t)(0+i0) + se^{i\varphi(t)}b(t)}{(1-s)b(t) + se^{i\varphi(t)}}, \quad (s, t) \in [0, 1] \times \mathbb{R} \quad (2)$$

where $\varphi(t)$ is quasi-periodic with constant 2π and quasi-period L . Indeed, this equation defines rational linear Bézier curves with control points $z = 0 + i0$ and $b(t)$ and associated weights $b(t)$ and $e^{i\varphi(t)}$. We denote $\varphi(t)$ as the tangent angle function since

$$\left(\frac{\partial p}{\partial s} \right) (0, t) = e^{i\varphi(t)}.$$

Consider the normal vector $n(t)$ of $b(t)$, which is given by

$$n(t) = -\text{sign}(r_\ell) e^{i\sigma_\ell(t)} \quad t \in [t_\ell, t_{\ell+1}).$$

The vector

$$u(t) = -\frac{b(t)\bar{n}(t)}{\bar{b}(t)}. \quad (3)$$

is the normal vector $n(t)$ reflected at the bisector of $b(t)$ and the origin, see Fig. 3 left. We use it to define the angle $\psi(t)$ such that

$$e^{i\psi(t)} = u(t). \quad (4)$$

More precisely, we choose the unique smooth quasi-periodic function $\psi(t) \in \arg u(t)$ with constant 2π and quasi-period L that satisfies

$$\psi(0) = \text{Arg } u(0) \in (-\pi, \pi].$$

The angles

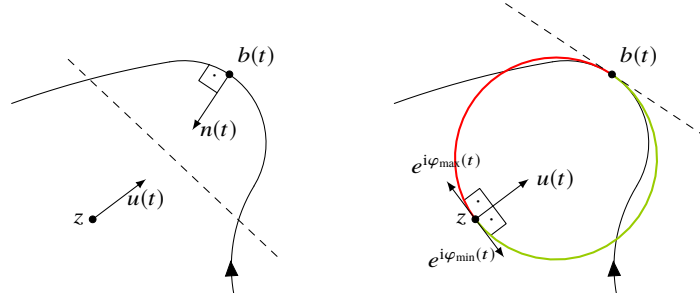


Fig. 3 Left: Boundary curve $b(t)$ (solid), its normal vector $n(t)$ and the reflected normal vector $u(t)$. Right: $\varphi_{\max}(t)$ and $\varphi_{\min}(t)$ specify the circular arcs that touch the boundary at $b(t)$

$$\varphi_{\min}(t) = \psi(t) - \frac{\pi}{2} \quad \text{and} \quad \varphi_{\max}(t) = \psi(t) + \frac{\pi}{2}$$

specify the two circular arcs that touch the boundary at $b(t)$, see Fig. 3 right. More precisely, the parameter lines $p(\cdot, t)$ represent these arcs if $\varphi(t) = \varphi_{\min}(t)$ or $\varphi(t) = \varphi_{\max}(t)$.

We summarize the main result of Jüttler et al. [7]:

Theorem 1 *The polar parameterization Eq. (2) is an arc fibration if and only if $\varphi(t)$ satisfies*

$$\varphi_{\min}(t) + 2k\pi < \varphi(t) < \varphi_{\max}(t) + 2k\pi$$

for some $k \in \mathbb{Z}$ and $\varphi'(t) > 0$ for all $t \in \mathbb{R}$.

Proof See Jüttler et al. [7], in particular Theorem 3 and Lemma 5. The proof also applies to the case of boundary curves that are only C^1 -smooth. \square

3 The φ -channel

We define the φ -channel Φ as the region in \mathbb{R}^2 that is above the lower boundary $\varphi_{\min}(t)$ and below the upper boundary $\varphi_{\max}(t)$:

$$\Phi = \{(t, \xi) \in \mathbb{R}^2 \mid \varphi_{\min}(t) < \xi < \varphi_{\max}(t)\}.$$

Figure 4 is an example of an arc domain (top) and its associated φ -channel (bottom). The graph shows the upper and lower boundary of one quasi period of Φ . The values of the knots t_ℓ are indicated by dashed vertical lines. Each b_ℓ has a unique color that corresponds to the color of Φ 's (lower and upper) boundary in the interval $[t_\ell, t_{\ell+1})$.

According to Theorem 1, the polar parameterization Eq. (2) is an arc fibration if and only if $\varphi(t)$ is monotonically increasing and its graph is contained in the

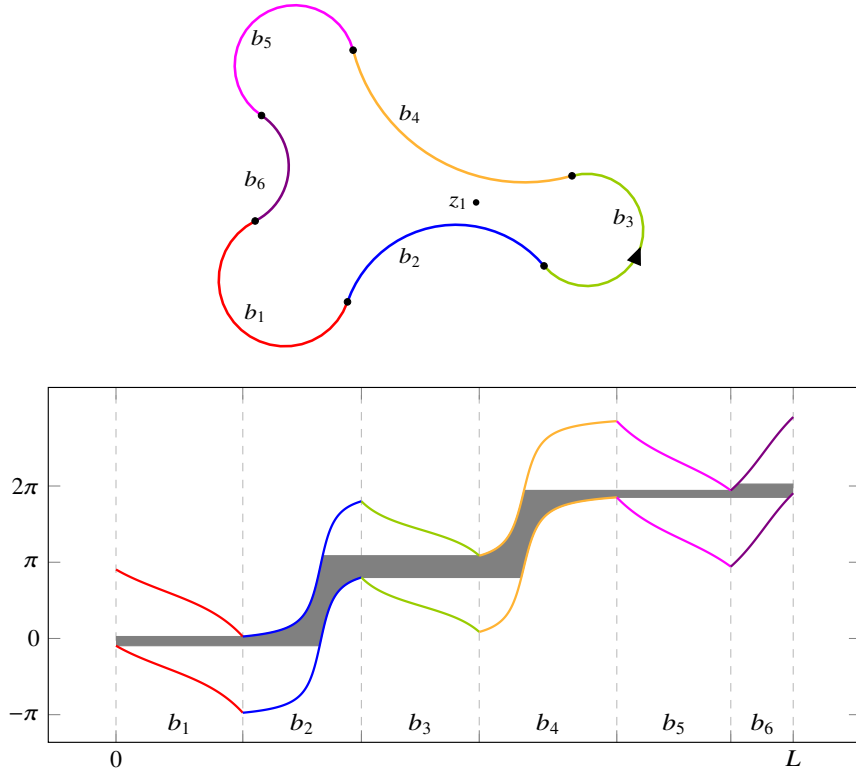


Fig. 4 The six arcs forming the arc domain from Fig. 2 (top) and the associated φ -channel (bottom) at the center z_1

φ -channel. This is only possible if the reduced φ -channel

$$\hat{\Phi} = \{(t, \xi) \in \mathbb{R}^2 \mid \max_{\tau \leq t} \varphi_{\min}(\tau) < \xi < \min_{\tau \geq t} \varphi_{\max}(\tau)\},$$

which is obtained by eliminating the upper and lower “pockets”, is connected. Fig. 4 shows the reduced φ -channel in gray.

We note that extremal points of the channel’s boundary appear at knots only:

Lemma 1 *The function $\psi(t)$, which specifies the direction of the reflected normal vector, is monotonic within each span $t \in (t_\ell, t_{\ell+1})$. More precisely,*

$$\text{sign } \psi'(t) = \text{sign}(r_\ell(|r_\ell| - |m_\ell|)), \quad t \in (t_\ell, t_{\ell+1}).$$

Proof A suitable scaling and rotation transforms the center of the ℓ -th circular arc into $m_\ell = 1$. We consider two cases:

- (I) $|r_\ell| = 1$: The arc passes through the origin, hence the reflected normal u is constant, which implies $\psi'(t) = 0$, see Fig. 5.

(II) $|r_\ell| \neq 1$: Evaluating the derivative $\psi'(t)$ with the assistance of Eq. (4) for the first equality and Eq. (3) for the second equality gives

$$\psi'(t) = -i\bar{u}u' = \frac{(r_\ell^2 - 1)\sigma'_\ell(t)}{(r_\ell + \cos \sigma_\ell(t))^2 + \sin^2 \sigma_\ell(t)}.$$

The denominator of the right-hand side is positive, and the first factor of the numerator satisfies

$$\text{sign}(r_\ell^2 - 1) = \text{sign}(|r_\ell| - |m_\ell|).$$

Moreover, condition (1) ensures that r_ℓ and $\sigma'_\ell(t)$ have the same signs.

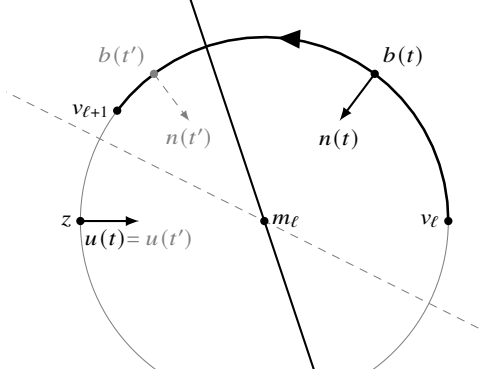


Fig. 5 The reflected normal vector is constant for $|r_\ell| = |m_\ell|$

We introduce the notion of discrete osculating circles, which will be useful for characterizing the connectivity of the reduced φ -channel:

Definition 2 A *discrete osculating circle* (DOC) at a joint v_ℓ is a circle that touches the boundary curve at v_ℓ while changing its side from the interior to the exterior of the domain Ω , or vice versa.

Each DOC possesses an orientation (which is specified by its radius) that is derived from the boundary curve at the point where it touches the boundary. We analyze the location of the possible centers m of DOCs, see Fig. 6: They form the line segment $\overline{m_{\ell-1}m_\ell}$ if the joint v_ℓ is not an inflection point. Otherwise, the possible centers of DOCs are all the other points on the line through $m_{\ell-1}$ and m_ℓ .

We say that the interior (exterior) of a circle with positive or negative radius lies to its left (right) or right (left), respectively.

Lemma 2 *There exists a DOC at v_ℓ through the center z of the parameterization if it is located on different sides of $b_{\ell-1}$ and b_ℓ .*

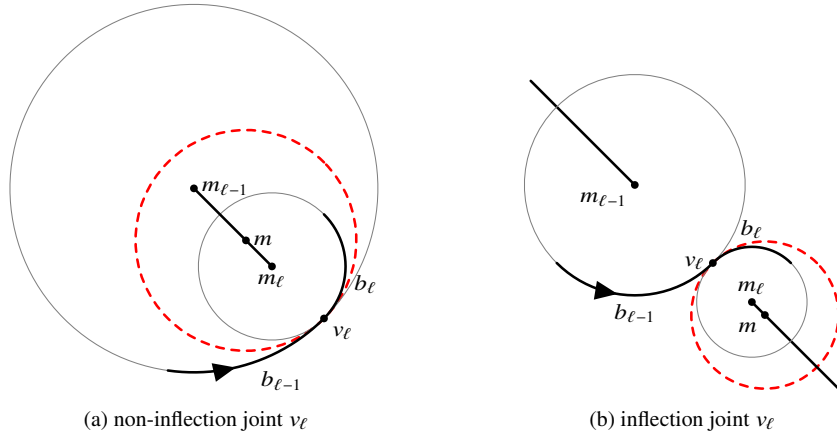


Fig. 6 The one parameter family of discrete osculating circles (dashed, red)

Proof This can be proved by analyzing the various cases defined by the signs and the differences of the radii $r_{\ell-1}$ and r_ℓ . See Fig. 7, which shows two of the six possibilities. The first case, as shown in (a), is characterized by $r_{\ell-1} > r_\ell > 0$. We assume that the center z lies left of $b_{\ell-1}$ and right of b_ℓ , i.e., within the gray region. We consider the DOCs at v_ℓ and let their centers m vary continuously from $m_{\ell-1}$ to m_ℓ . By varying m , the associated DOCs sweep the entire gray area. Thus, if z is located within the swept area, there exists a point m_z on $\overline{m_{\ell-1}m_\ell}$, which is the center of a DOC at $v_\ell = b(t_\ell)$. The remaining five cases can be dealt with similarly. \square

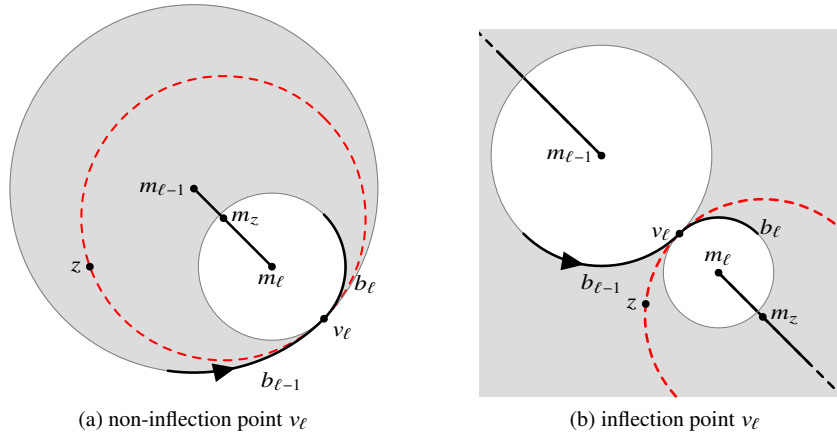


Fig. 7 The discrete osculating circle (dashed) with center m_z passes through the center z

The function $\psi(t)$ possesses a *stationary point* at t_ℓ if $\psi'(t) \leq 0$ for $t \in [t_{\ell-1}, t_\ell)$ and $\psi'(t) \geq 0$ for $t \in [t_\ell, t_{\ell+1})$, or vice versa.

Lemma 3 *The function $\psi(t)$ possesses a stationary point at t_ℓ if a DOC at v_ℓ passes through the center z of the parameterization.*

Proof We consider the case where the DOC through z at v_ℓ lies left of $b_{\ell-1}$ and right of b_ℓ (cf. Lemma 2). Then $|r_{\ell-1}| > |m_{\ell-1}|$ (see Fig. 7) and $\psi(t)$ is monotonically increasing for $t \in [t_{\ell-1}, t_\ell)$, according to Lemma 1. Analogously, one can verify that $\psi'(t) < 0$ for $t \in [t_\ell, t_{\ell+1})$. Therefore $\psi(t)$ has a local maximum at $t = t_\ell$. A local minimum is obtained if the DOC at v_ℓ through z lies right of $b_{\ell-1}$ and left of b_ℓ . \square

We remark that the monotonicity properties of $\psi(t)$ (Lemma 1) are inherited by the functions $\varphi_{\min}(t)$ and $\varphi_{\max}(t)$. This fact is also illustrated in Fig. 4.

Two curves are said to be in *oriented anti-contact* if they touch each other with opposite orientation.

Lemma 4 *If a minimum $\varphi_{\max}(t_k)$ of the upper boundary and a maximum $\varphi_{\min}(t_\ell)$ of the lower boundary satisfy $\varphi_{\max}(t_k) = \varphi_{\min}(t_\ell)$ then there exist DOCs at v_k and v_ℓ that are in oriented anti-contact at the center z .*

Proof Since both extrema have equal ordinates we observe that

$$\begin{aligned} 0 &= \varphi_{\max}(t_k) - \varphi_{\min}(t_\ell) \\ &= \psi(t_k) - \psi(t_\ell) + \pi, \end{aligned}$$

which means that the difference $\psi(t_k) - \psi(t_\ell)$ is equal to π . Therefore the reflected normal vectors $u(t_k)$ and $u(t_\ell)$ are anti-parallel, i.e., $u(t_k) = -u(t_\ell)$ and the DOCs through the center z at v_k and v_ℓ touch. We conclude this proof by noting that the DOCs at v_k and v_ℓ through z are in oriented anti-contact since the reflected normal vectors point to their left. \square

4 The arc fibration kernel

We say that the φ -channel is *disconnected* if there exists no strictly increasing function $\varphi(t)$ through Φ . Given an arc domain Ω , we consider varying locations of the center z . We are interested in situations that lead to connected φ -channels:

Definition 3 The arc fibration kernel K of an arc domain Ω is the set of all centers in Ω for which an arc fibration exists.

$$K(\Omega) = \{z \in \Omega \mid z \text{ admits an arc fibration}\}$$

The transition case between locations of the center z that correspond to connected and disconnected φ -channels is characterized by the assumptions of Lemma 4 and, additionally $t_\ell < t_k$: Indeed, since $\varphi(t) \in \Phi$ satisfies $\varphi(t_\ell) \geq \varphi_{\min}(t_\ell)$ and

$\varphi(t_k) \leq \varphi_{\max}(t_k)$, there must be an interval in $[t_\ell, t_k]$ where $\varphi(t)$ is constant or decreasing.

We identify the locations of the centers z that correspond to transition cases:

Lemma 5 *The points of oriented anti-contact of DOCs at two joints v_k and v_ℓ are located on a circle.*

Proof The G^1 interpolation of a pair of point-tangent pairs, $(v_k, b'(t_k))$ and $(v_\ell, b'(t_\ell))$ using two smoothly joined circular arcs is known as biarc interpolation. For each such pair there is a one parameter family of points at which these two circular arcs touch. The touching points are located on a circle – the so called joint circle, see Šír et al. [9] for a proof. Since we consider DOCs that are in oriented anti-contact, one of the tangents has to be inverted, i.e., we use $(v_k, b'(t_k))$ and $(v_\ell, -b'(t_\ell))$ for the biarc interpolation. \square

The *anti-joint circle* (AJC) of two joints v_k and v_ℓ is the circle formed by the oriented anti-contact points, see the previous lemma. An example is shown in Fig. 8. For any center z located on the AJC we obtain, two pairs (red and blue) of DOC arcs

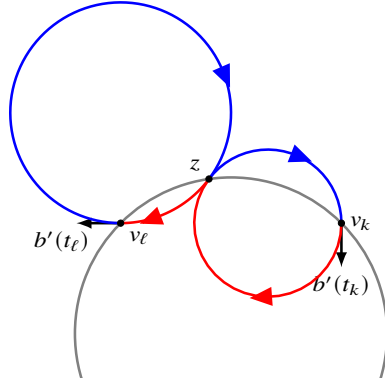


Fig. 8 There are two paths (red and blue) which connect v_k and v_ℓ along any z on the anti-joint circle (gray)

with opposite orientation touching at z . It should be noted that the information about these arcs depends on the domain boundary and cannot be derived solely from the point tangent pairs $(v_k, b'(t_k))$ and $(v_\ell, b'(t_\ell))$. As shown in Fig. 8, there are always two possible DOC arc pairs, but at most one of them is valid, see Fig. 10 the red valid path. This discussion will be continued when describing the orientation filter in the next section.

Theorem 2 *The boundary of the arc fibration kernel $\partial K(\Omega)$ of an arc domain consists of arcs of anti-joint circles and of the domain boundary.*

Proof This follows from the definition of the arc fibration kernel and from Lemmas 4 and 5. \square

Figure 9 shows the subdivision of the plane, which is defined by the anti-joint circles of the arc domain from Fig. 4. The φ -channel for a valid center point z_1 of

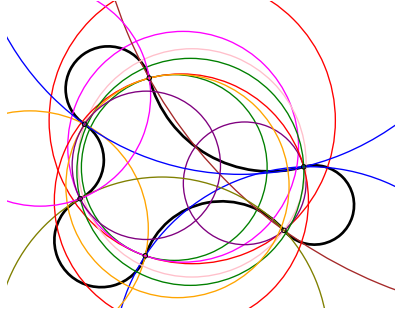


Fig. 9 The anti-joint circles (shown in different colors) of the arc domain from Fig. 2 (black)

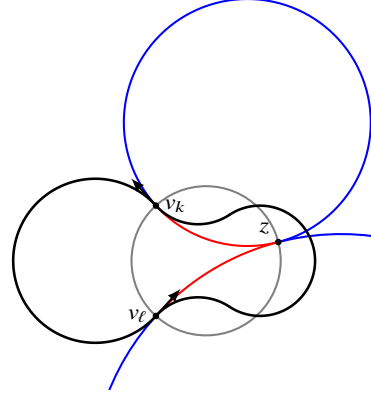


Fig. 10 The anti-joint circle (gray) of two joints

the parameterization is depicted in Fig. 4 (bottom). In addition, we visualize the φ -channels for invalid centers (z_2 and z_3) taken from adjacent faces of the subdivision in Fig. 11.

5 Kernel computation

Based on Theorem 2 we formulate a method to compute the arc fibration kernel for a given arc domain that consists of n circular arcs. We compute a super-set of the kernel's boundary. Inactive components are eliminated by trimming and by applying various filters, which we will describe later in this section.

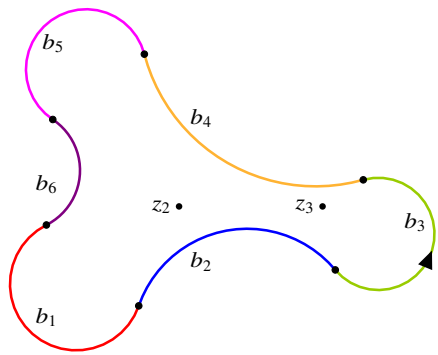
Algorithm 1 is an outline of our method. We initialize \mathcal{Z} to be the empty set and use it to collect arcs that may contribute to the kernel's boundary.

The main loop of the algorithm iterates over the set of pairs

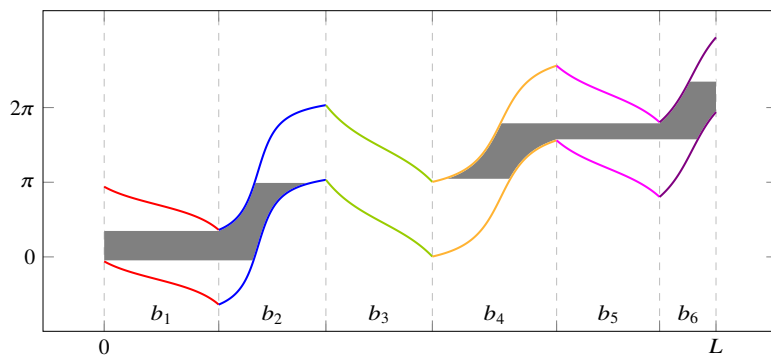
$$P = \{(v_k, v_\ell) \mid k, \ell = 1, \dots, n \text{ for } k < \ell\},$$

which has $O(n^2)$ elements. Each iteration considers a particular pair $(v_k, v_\ell) \in P$ and performs four operations, which are listed below. Further details will be presented in the subsequent text.

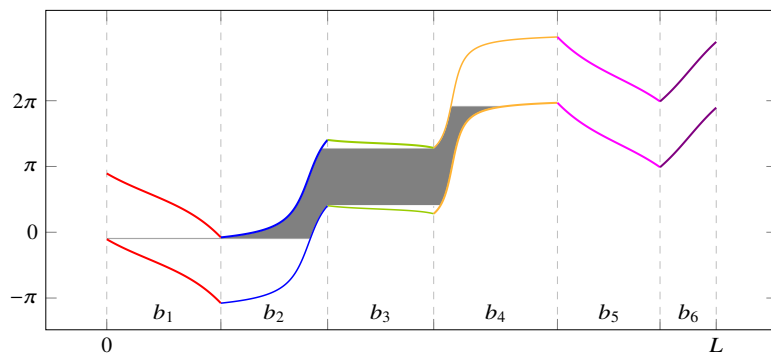
- i) We create the set of contributing arcs (*sca*) and initialize it with the *anti-joint circle* (Line 4).
- ii) *Trimming* (Line 5) is applied to *sca*. After this operation, *sca* consists of zero, one or two arcs.



(a) The sixCircles example



(b) Center z_2



(c) Center z_3

Fig. 11 Reduced φ -channels for two centers

Algorithm 1: Arc fibration kernel

```

Input: Arc spline  $b(t)$ 
Output: Arc fibration kernel  $K(\Omega)$ 
1 Initialize  $\mathcal{Z}$  as the empty set.
2 for  $k = 1, \dots, n - 1$  do
3   for  $\ell = k + 1, \dots, n$  do
4     Create the anti-joint circle  $ajc$  associated with the pair  $(v_k, v_\ell)$  and initialize  $sca$ .
5     Trim the  $sca$ .
6     Apply the orientation filter to  $sca$ .
7     Apply the pear filter to  $sca$  and augment arcs by side information.
8     Add  $sca$  to  $\mathcal{Z}$ . /* nothing is added if  $sca = \emptyset$  */
9   end
10 end
11 Extract the kernel using  $\mathcal{Z}$  and  $b(t)$ .

```

- iii) The *orientation filter* (Line 6) removes arcs of sca with non-matching orientations of the associated DOCs.
- iv) The *pear filter* (Line 7) identifies and removes a specific type of arcs from sca which are known not to contribute to $\partial K(\Omega)$.

The resulting set sca is added to \mathcal{Z} . Clearly, the trimming and the two filters may result in an empty sca . In that case we proceed to the next element of P . Finally, we extract the arc fibration kernel using the potential kernel boundary arcs \mathcal{Z} and $b(t)$.

Anti-joint circle Recall that all oriented anti-contacts of DOCs lie on anti-joint circles, see Lemma 5. The center of the AJC for (v_k, v_ℓ) can be computed as the intersection of two bisectors: The first one is defined by v_k and v_ℓ , and the second one by the two points $v_k + b'(t_k)$ and $v_\ell - b'(t_\ell)$. The radius of the AJC is the distance from its center to v_k .

We initialize sca with the anti-joint circle. Each element of sca stores its center, radius, angular range (which is initialized with the full circle) and a pointer to the associated pair $(v_k, v_\ell) \in P$. The range is needed to identify particular arcs on the AJC, which are created by the (following) trimming step.

Trimming The restriction of possible centers of DOCs (cf. Definition 2) results in a restriction of possible oriented anti-contact points on the AJC. The trimming procedure sets sca to be those arcs of the AJC in which every center point z (of the parameterization) corresponds to two DOCs, i.e., the DOC's center point restrictions are met. Each of two systems of DOCs at v_ℓ and v_k defines an angular range for the points on the AJC. The intersection of these two ranges results in zero, one or two ranges that are included into the sca .

Figure 12 illustrates the DOCs at v_k (green) and v_ℓ (red) together with their centers on the dashed lines. The points of oriented anti-contact on the AJC lie on the blue arc. In this example sca is the blue arc after trimming.

Orientation filter Given a point z on an arc of the sca , we consider the two DOCs defined by it. Each of them splits into two arcs that connect z with the associated

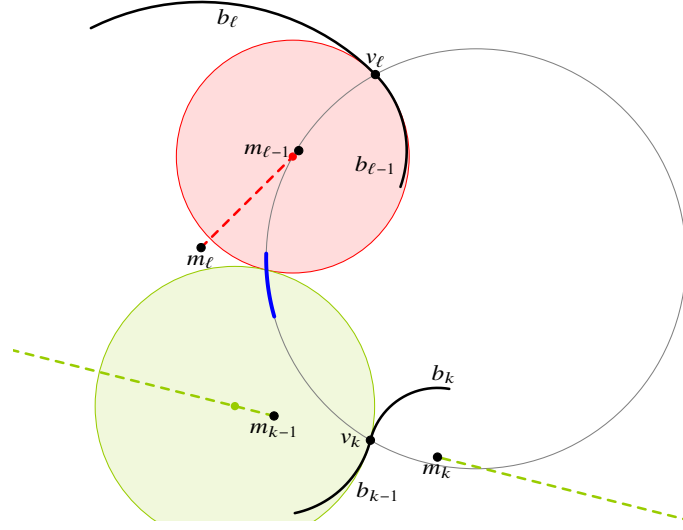


Fig. 12 The anti-joint circle's valid arc (blue) with respect to v_k and v_{ℓ}

points v_{ℓ} and v_k on the boundary. These four arcs form two possible paths (red and blue of Fig. 8) that connect v_{ℓ} and v_k and are compatible with the orientations of the DOCs.

Now we analyze the behavior of these paths with respect to the domain boundary in the vicinity of v_{ℓ} and v_k . A path is valid, if it enters the domain at its starting point, and it approaches the domain boundary from the interior at its end point, see Fig. 13a. Otherwise a path is said to be invalid, see Figs. 13b to 13d. We say that a valid path is formed by an entering and a leaving arc.

The two possible paths are either both invalid, or one of them is valid and the other one is invalid. We filter out configurations without a valid path. For this, it suffices to analyze a test point on each arc of sca , e.g. its midpoint. Depending on the geometry of the domain boundary in the vicinity of v_{ℓ} and v_k we either find a valid path (either the red one or the blue one) or we filter out the arc of the sca under consideration.

Summing up, we loop over all arcs ρ of sca and perform three actions: First, a test point z on ρ is chosen. Second, we construct the DOCs that are in oriented anti-contact at z and their two paths. Third, we remove ρ from sca if there is no path that consists of an entering and a leaving arc.

Pear filter We consider a test point z on an arc of sca and its two associated DOCs at v_k and v_{ℓ} . This configuration characterizes a transition case between connected and unconnected $\hat{\Phi}$ under the assumptions of Lemma 4 and $t_k > t_{\ell}$. We refer to this configuration as *sting* case, see Fig. 14 (right). However, z is not a transition point if $t_k < t_{\ell}$. The latter configuration is referred to as *pear* case, see Fig. 14 (left). In a pear case the arc on which the test point is located may be removed from the sca .

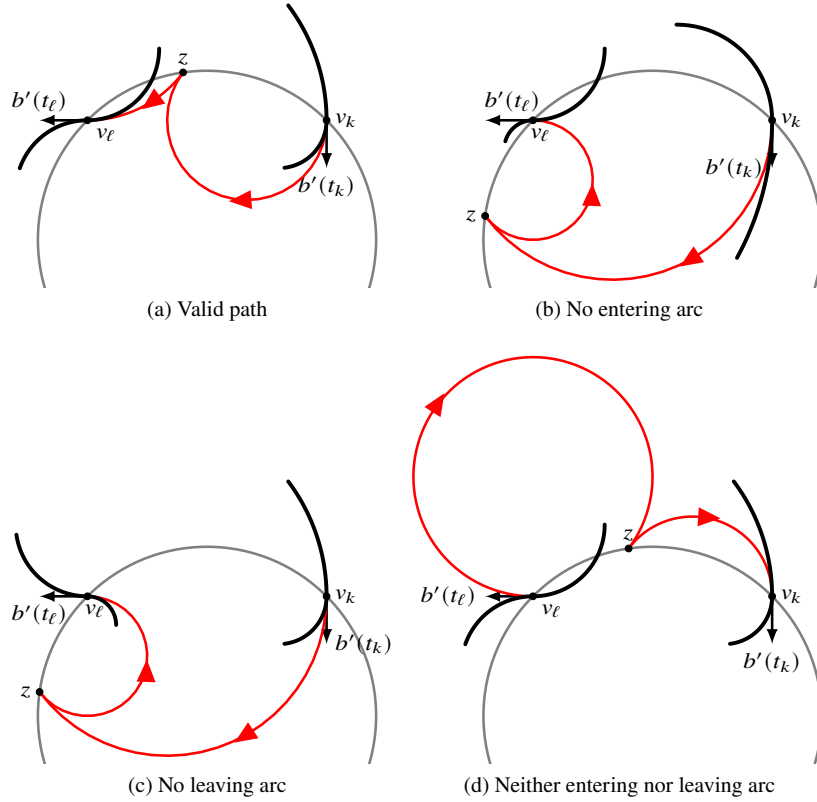


Fig. 13 Various configurations of entering and leaving arcs

We handle pear cases by performing three operations on all arcs ρ of sca (Algorithm 2). First, we choose a test point z (e.g. the arc's midpoint) and compute the corresponding path. Note that there is exactly one path that connects v_k and v_ℓ . We denote the signed radius of the entering arc by r_{in} and the signed radius of the leaving arc by r_{out} . After obtaining those two radii we determine the type of the configuration with Table 1, which provides criteria on r_{in} and r_{out} to identify pear (and sting) cases. If a pear case is determined, we remove ρ from sca .

The choice of the test point z on ρ is arbitrary. While different choices of z result in different signs and absolute value of r_{in} and r_{out} , it does not change the classification in pear and sting cases. We discuss the effects of relocating z on the signs of DOC radii. The classification depends on the signs of the DOCs radii and their absolute values.

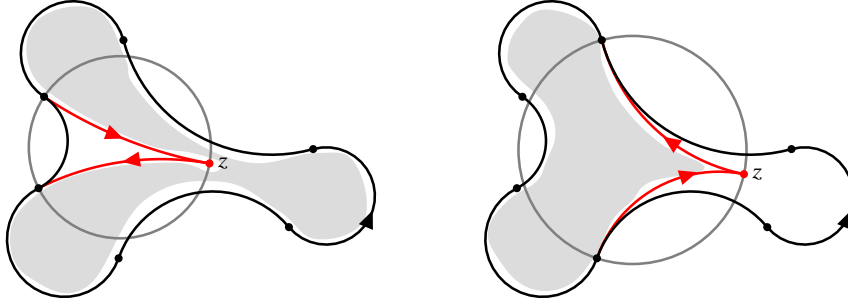


Fig. 14 Pear (left) and sting (right) case

Algorithm 2: Pear filter

Input: Set of contributing arcs sca
Output: The pear filtered sca

```

1 foreach  $\rho$  in  $sca$  do
2   | Choose a test point  $z$  on  $\rho$ .
3   | Create the to  $z$  associated path and compute the DOC arc's radii.
4   | if  $z$  constitutes a pear case then
5   |   | Remove  $\rho$  from  $sca$ .
6   | else
7   |   | Augment  $\rho$  with arc fibration kernel side information.
8   | end
9 end

```

Table 1 Pear filter

		sign r_{in}	
		1	-1
sign r_{out}	1	pear	$ r_{out} > r_{in} $ sting $ r_{out} < r_{in} $ pear
	-1	$ r_{out} > r_{in} $ pear $ r_{out} < r_{in} $ sting	sting

- The radius of a DOC cannot change its sign by going over zero due to their definition and the fact that the boundary curve does not consist of circular arcs with radius zero.
- The radius of a DOC can change its sign by going over infinity: The value of a DOC's radius might increase (decrease) to ∞ ($-\infty$) and come back with opposite sign. These changes lead always to the same classification. Consider for instance the pear case in which $|r_{out}| > |r_{in}|$. Moving z may result in r_{out} approaching minus infinity and then back with positive radius at which point both radii are positive and the classification according to Table 1 remains pear.

- We consider the transition case in which DOC's radii have opposite signs but equal absolute value. The DOC's centers are then identical, which means that v_k, v_ℓ are located on the DOC and their tangents are tangents of the DOC. We do not examine this case since it has probability zero (i.e. it is non-generic).

All six cases portrayed in Table 1 are illustrated in Fig. 15. We discuss the two cases of the left column in more detail.

The example on the top left illustrates a pear case configuration. The black arrow indicates the orientation of the boundary from which the entering and the leaving arcs (red) inherit their orientations. The point of oriented anti-contact is z and the gray circle is the anti-joint circle. Intuitively it is clear that an entering and a leaving arc still exists if we move z within a small neighborhood of its current position. The arc on which z is located is therefore not in $K(\Omega)$.

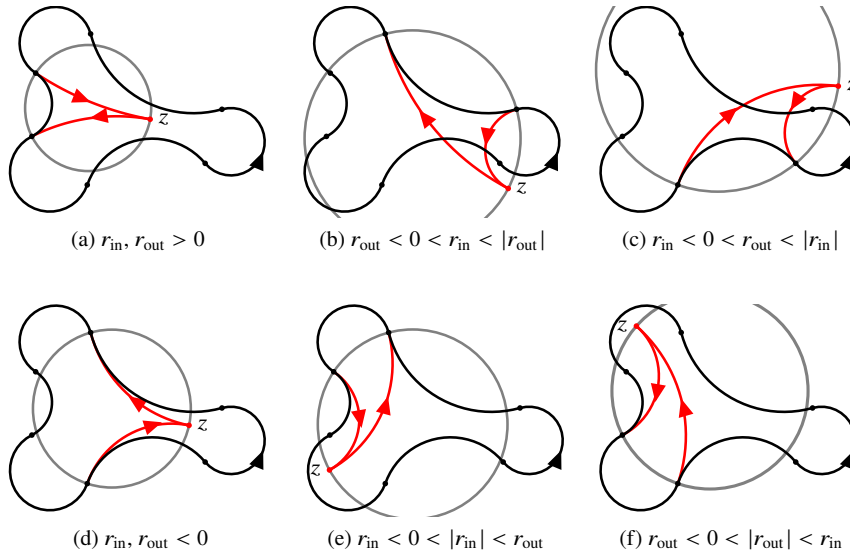


Fig. 15 Illustrations of pear (top row) and sting (bottom row) cases according to Table 1

A sting case is illustrated on the bottom left of Fig. 15. One may observe that a valid path can be obtained if we move z to the left. However, no valid path exists if z is moved to the right. Clearly, that arc of *sca* must not be deleted by the pear filter since it might belong to $K(\Omega)$.

Remark 1 Although arcs of *sca* that form sting cases are not deleted, their detection is beneficial since the side of the arc on which the arc fibration kernel lies can be identified.

Kernel extraction Due to the local nature of the trimming and filter procedures, which we discussed above, there may still be arcs which do not contribute to the

kernel's boundary. Therefore we need an additional step to extract the kernel: We consider the planar circular subdivision of Ω that is induced by \mathcal{Z} . Elements of \mathcal{Z} outside of Ω are ignored.

We consider the directed dual graph DG of the planar circular subdivision. The direction of an edge is the side on which the kernel is located, see Fig. 16. A *sink* is a node of a graph, whose edges are directed towards itself. All faces of the subdivision, which potentially belong to $K(\Omega)$, are identified as sinks of DG . For each sink we choose a test point z on the corresponding face and compute the associated reduced φ -channel $\hat{\Phi}$. The face is part of the kernel $K(\Omega)$ if $\hat{\Phi}$ is connected.

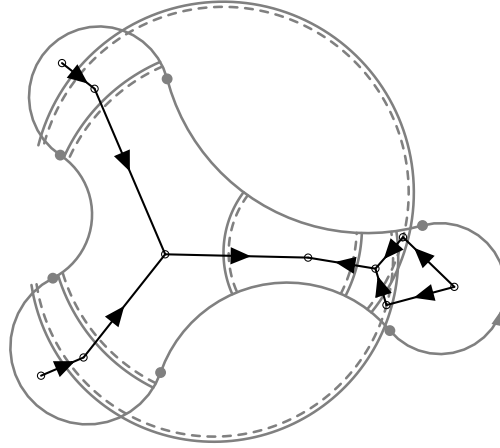


Fig. 16 Dual graph of the planar subdivision of Ω induced by arcs of anti-joint circles

Computational complexity We analyze the time complexity of Algorithm 1 in two steps. First, the main loop iterates over all $N = \binom{n}{2}$ pairs of joints. All procedures within that loop entail only modifications on sca and have constant complexity.

Second, the planar circular subdivision of the kernel extraction procedure is constructed in $O(N \log N + k)$ time (cf. [5]) with k being the number of intersections between the elements of \mathcal{Z} ($|\mathcal{Z}| \leq 2N$). The complexity of the dual graph DG is $O(N + k)$. We determine in $O(n)$ time whether a face, which corresponds to a sink of DG , is in the arc fibration kernel.

The analysis of the space complexity consists of two parts: First, the main loop can be implemented in such a way that it only requires storage in the size of the kernel's boundary, which is typically $O(n)$ as we will demonstrate in Section 6. However, in the worst case, space can become quadratic in n . Second, the kernel extraction requires $O(N + k)$ space, see [5].

Finally we note that the time and space complexity analysis is very pessimistic. In practice, Algorithm 1 runs in $O(n^2)$ time and linear space.

6 Experimental results and examples

We apply our algorithm to the `sixCircles` example Fig. 17: The boundary is shown as black solid bold line and consists of six circular arcs. In the top left figure all 15 (complete) *sca*s are shown. The results after trimming are shown on the top right. The application of the orientation filter (bottom left) further reduces the number of *sca* elements. Finally, the pear filter reduces the number of *sca* arcs once more and augments them with an orientation indicating the side of the kernel (dashed arcs).

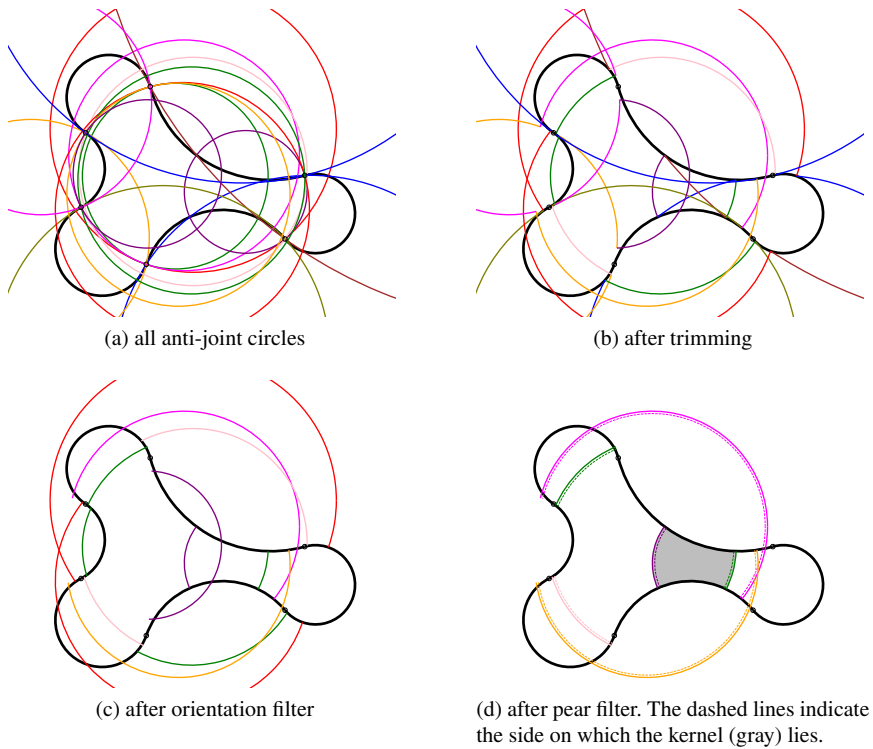


Fig. 17 The `sixCircle` example at various stages of Algorithm 1. The black curve is the boundary of the arc domain Ω

Figure 18 shows the result of our algorithm applied to the `sixCircles` example together with three center points of the parameterization: The center z_1 is located in the interior of the kernel and its associated reduced φ -channel is therefore connected, see Fig. 4. The centers z_2 and z_3 are both in the exterior of the arc fibration kernel and their $\hat{\Phi}$'s are disconnected, cf. Figs. 11b and 11c.

We study the behavior of Algorithm 1 for the two domains, `hourGlass` (top row) and `waveGlass` (bottom), shown in Fig. 19. The kernels of the three examples are

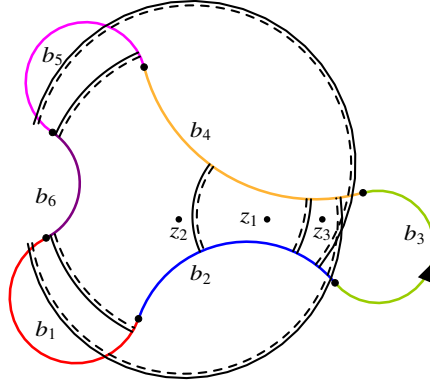


Fig. 18 The arc fibration boundary with three center points z_1 , z_2 and z_3

shaded in gray and labeled with $K(\Omega)$. The boundary of the `hourGlass` example is an approximation of a spline curve by an arc spline. On the left, 48 circular arcs are used to approximate the spline and 216 circular arcs on the right. One may notice that the size of the induced subdivision grows linearly, the number of intersections among arcs of \mathcal{Z} seem to stay constant.

Figure 20 shows the (initial) quadratic number of elements in \mathcal{Z} (blue) and after applying trimming and the two filters to the `hourGlass` example. Trimming (red) leaves most *scas* empty and only a linear number of *scas* remain in \mathcal{Z} . The orientation and pear filter further reduce the size of \mathcal{Z} . The dashed reference lines indicate linear and quadratic complexity. An analogous analysis holds for the `waveGlass` example.

Clearly, it is possible that the arc fibration kernel is empty, see Fig. 22.

7 Conclusion

The main contribution of this paper is twofold: First, we defined arc fibrations of arc domains and showed that the kernel's boundary consists solely of circular arcs, with the help of discrete osculating circles. Second, the proposed algorithm massively reduces the number of potential boundary elements (from initially $O(n^2)$) of the kernel by using local features (e.g. trimming, orientation filter and pear filter). The algorithm is easy to implement, uses only elementary data structures and its parallelization is straightforward. Note that the algorithm, unlike the theoretical part in Section 2, does not make use of the parameterization of $b(t)$, it uses only the sequence of boundary arcs.

The location of the parameterization's center point may be subject to optimization since we compute the entire kernel of the domain, i.e., we may choose the center point that is most suitable for a specific application. The investigation of suitable optimality criteria could be of interest.

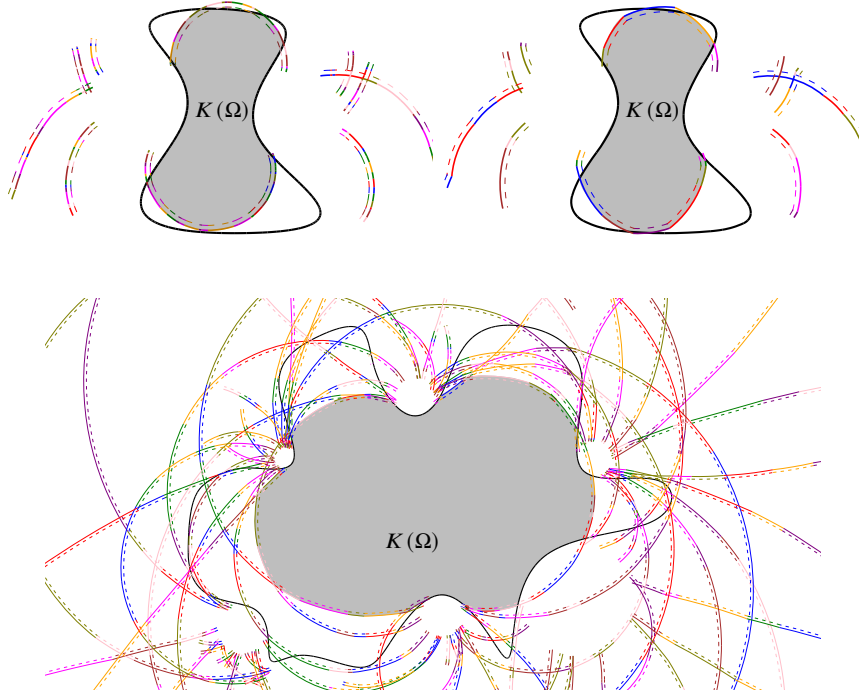


Fig. 19 The hourGlass (top row) and waveGlass (bottom) examples. Different colors indicate different anti-joint circle arcs

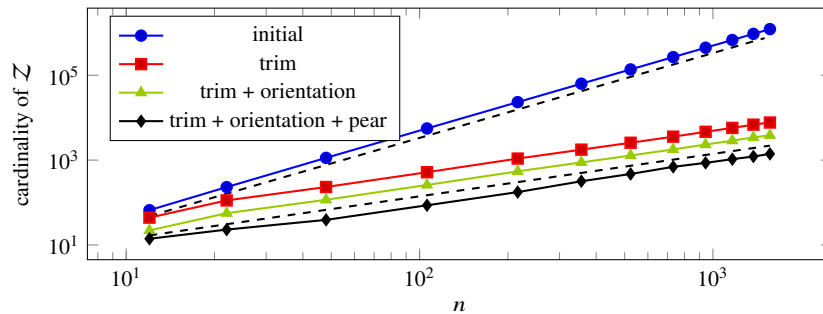


Fig. 20 Size of \mathcal{Z} (initial value and after applying the various filters) for varying size n of the input arc spline hourGlass. The dashed lines indicate quadratic and linear complexity

Our numerical experiments indicate that the algorithm's run-time is influenced by the number of curvature extrema. It should be interesting to develop an algorithm with lower than quadratic complexity. It is well known (e.g. [11, 12]) that splines can be approximated by arc splines that preserve spirals and therefore the number

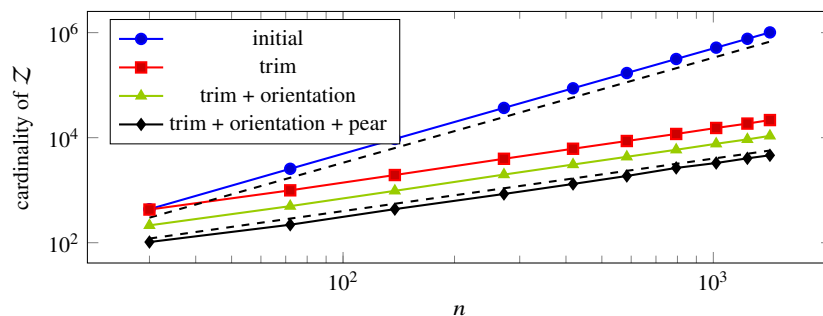


Fig. 21 Size of Z (initial value and after applying the various filters) for varying size n of the input arc spline waveGlass. The dashed lines indicate quadratic and linear complexity

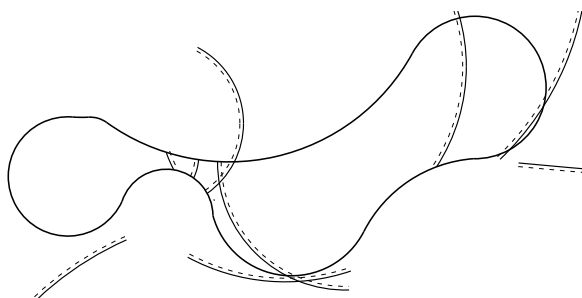


Fig. 22 This domain has an empty arc fibration kernel

of curvature extrema. Other interesting problems for future investigations are the extension to 3D and the analysis of fibrations with more general parameter lines, such as (low degree) Bézier curves (cf. [10]) and conic sections.

References

1. Aichholzer, O., Aigner, W., Aurenhammer, F., Hackl, T., Jüttler, B., Rabl, M.: Medial axis computation for planar free-form shapes. *Computer-Aided Design* **41**(5), 339–349 (2009)
2. Aichholzer, O., Aurenhammer, F., Hackl, T., Jüttler, B., Rabl, M., Šír, Z.: Computational and structural advantages of circular boundary representation. *International Journal of Computational Geometry & Applications* **21**, 47–69 (2011)
3. Avis, D., Toussaint, G.: An efficient algorithm for decomposing a polygon into star-shaped polygons. *Pattern Recognition* **13**(6), 395–398 (1981)
4. Dobkin, D.P., Souvaine, D.L.: Computational geometry in a curved world. *Algorithmica* **5**(1), 421–457 (1990)
5. Halperin, D., Sharir, M.: Arrangements. In: C.D. Tóth, J. O'Rourke, J.E. Goodman (eds.) *Handbook of Discrete and Computational Geometry*, chap. 28, pp. 723–762. Chapman and Hall/CRC (2017)

6. Icking, C., Klein, R.: Searching for the kernel of a polygon – a competitive strategy. In: Proceedings of the eleventh annual Symposium on Computational Geometry, pp. 258–266. ACM (1995)
7. Jüttler, B. and Maroschek, S. and Kim, M.-S. and Hong, Q.Y.: Arc fibrations of planar domains. *Computer Aided Geometric Design* **71**, 105–118 (2019)
8. Lee, D.T., Preparata, F.P.: An Optimal Algorithm for Finding the Kernel of a Polygon. *Journal of the ACM (JACM)* **26**(3), 415–421 (1979)
9. Šír, Z., Feichtinger, R., Jüttler, B.: Approximating curves and their offsets using biarcs and Pythagorean hodograph quintics. *Computer-Aided Design* **38**(6), 608–618 (2006)
10. Trautner, S., Jüttler, B., Kim, M.-S.: Representing planar domains by polar parameterizations with parabolic parameter lines. *Computer Aided Geometric Design* **85**, 101966 (2021)
11. Walton, D.J., Meek, D.S.: A planar cubic Bézier spiral. *Journal of Computational and Applied Mathematics* **72**(1), 85–100 (1996)
12. Walton, D.J., Meek, D.S.: Approximation of a planar cubic Bézier spiral by circular arcs. *Journal of Computational and Applied Mathematics* **75**(1), 47–56 (1996)
13. Weiß, B., Jüttler, B., Aurenhammer, F.: Mitered offsets and skeletons for arc polygons. *International Journal of Computational Geometry & Applications* **30**(03-04), 235–256 (2020). Published in 2021
14. Zubè, S.: A circle representation using complex and quaternion numbers. *Lithuanian Mathematical Journal* **46**(2), 246–255 (2006)